DOI: 10.26599/FSHW.2024.9250216

Contents lists available at SciOpen

Food Science and Human Wellness

journal homepage: https://www.sciopen.com/journal/2097-0765

Inonotus obliquus polysaccharides prevent UVB-induced skin photodamage by modulating Sirt3-activated Foxo3a/PINK1-Parkin pathway: an *in vitro* and *in vivo* study

Pei Lin[#], Yin-ying Lu[#], Hong-yu Shi, Zhen-dong Chen, Jun Lin[*]

School of Life Sciences and Health Engineering, Jiangnan University, Wuxi 214122, China

ABSTRACT: *Inonotus obliquus*, an edible and medicinal fungus, has proven to be beneficial for relieving body aging. Previous research has shown that *Inonotus obliquus* polysaccharide (IOP) can effectively reduce oxidative stress and alleviate photoaging in UVB-treated HaCaT cells. However, the underlying mechanism is still unclear. This study aimed to investigate the mechanism through which IOP mitigates skin photodamage by modulating mitochondrial autophagy through both *in vivo* and *in vitro* experiments. The results indicated that IOP alleviated the thickening of the stratum corneum and inflammatory infiltration caused by UVB radiation. Moreover, IOP effectively inhibited the mRNA expression of MMP1 and MMP3 to prevent collagen breakdown and decreased the expression of aging-related proteins (P53 and P21) and inflammatory factors (TNF-α and IFN-γ) in UVB-induced mice. Both *in vitro* and *in vivo* studies demonstrated that IOP increased Sirt3 expression, activated the Foxo3a/PINK1-Parkin pathway and enhanced mitochondrial autophagy to reduce photodamage. Additionally, IOP could regulate the gut microbes in photodamaged mice and increase the relative abundance of *Clostridium_XlVa*, *Desulfovibrio*, and *Barnesiella*, which are important for protecting the intestinal barrier and alleviating intestinal dysfunction. These results provide a theoretical foundation for the use of IOP as a natural component to reduce skin photodamage.

Key words: *Inonotus obliquus* polysaccharides, mitophagy, Sirt3, photodamage

1. Introduction

Long-term exposure to UVB radiation can lead to skin inflammation, DNA damage, oxidative stress, and collagen fiber degradation, ultimately resulting in skin photodamage[1-3]. Mitochondria, which are organelles responsible for aerobic respiration and cellular energy metabolism, play a crucial role in maintaining cellular homeostasis[4, 5]. UVB radiation disrupts the normal functioning of mitochondria in HaCaT cells, resulting in decreased ATP levels, loss of mitochondrial membrane potential, and dysfunctional mitochondrial aggregation[6]. Mitochondrial dysfunction induces cellular senescence, chronic inflammation, and an increase in reactive oxygen species[7, 8]. To maintain mitochondrial and intracellular homeostasis, cells selectively remove damaged mitochondria through mitophagy [9]. Research has demonstrated that inducing mitochondrial

[#] The first two authors contributed equally to this article.
***Corresponding author**
junlin@jiangnan.edu.cn

Received 30 November 2023
Received in revised from 8 January 2024
Accepted 10 March 2024

autophagy can enhance the collagen content and antioxidant capacity in the skin of aging rats[10]. These findings suggested that restoring mitochondrial function is essential for reversing skin aging.

Sirtuin-3 (Sirt3) regulates mitochondrial metabolism, strengthens antioxidant defense, and contributes to cellular aging and tumor development. It serves as a crucial target for the treatment of mitochondrial dysfunction diseases[11, 12]. Sirt3 deacetylates Forkhead box O3 (Foxo3a), leading to its activation[13]. This deacetylation of Foxo3a then activates the mitochondrial autophagy gene PTEN-induced putative protein kinase (PINK1), which regulates mitochondrial autophagy[14]. The Sirt3-foxo3a/PINK1-E3 ubiquitin ligase protein (Parkin) signaling pathway has been demonstrated to be involved in various diseases, such as myocardial damage caused by diabetes, heart failure, and degenerative diseases[15-17]. Sirt3 is an important target for treating mitochondrial dysfunction diseases, and its signaling pathway is a crucial component of antioxidant stress and cytoprotective mechanisms[13, 18, 19]. Regulating mitochondrial function through Sirt3 is also expected to have a significant impact on the prevention and treatment of skin photodamage.

Inonotus obliquus is a widely distributed medicinal and edible fungus found in North America, Asia and Europe. It is commonly used in folk medicine due to its various biological activities, including antioxidant, anticancer, anti-inflammatory, and immunoregulatory properties[20, 21]. Polysaccharides are one of the main biological components of *Inonotus obliquus* and exhibit antiviral, antioxidant, hypolipidemic, and hypoglycemic effects[22]. Our previous research demonstrated that *Inonotus obliquus* polysaccharide (IOP) can effectively prevent UVB-induced skin photoaging[23, 24]. These findings also suggested that IOP may have a regulatory effect on mitochondria, although the specific mechanism involved is still unclear. In this study, we aimed to investigate whether IOP can alleviate skin photodamage by modulating mitochondrial autophagy through both *in vivo* and *in vitro* experiments. The results of this study will provide an experimental basis for the further development and utilization of *Inonotus obliquus* in the functional food and cosmetics industries.

2. Materials and methods

2.1 Preparation of IOP

The *Inonotus obliquus* fruiting body was crushed and then subjected to water extraction and alcohol precipitation to prepare the IOP. Purified polysaccharides were obtained by using the Sevage reagent (chloroform: n-butanol = 4:1) to remove protein impurities. High performance liquid chromatography (HPLC) analysis revealed that the monosaccharide composition of IOP included Mannose, Glucosamine, L-rhamnose monohydrate, Glucuronic acid, D-Galacturonic acid, Glucose, D-galactose, Xylose, L-Arabinose and Fucose[24].

2.2 Animal treatment and UVB irradiation

Forty 8-week-old female C57BL/6 mice weighing 17-20 g were used in this study. The mice were purchased from Vital River, Beijing and housed in IVC crates maintained at a constant temperature (20-26℃) and humidity (40%-60%). All animal experimental protocols were approved by the Laboratory Animal

Management and Animal Welfare Ethics Committee of Jiangnan University (Approval Number: JN.NO20220930c0401230[399]).

After one week of adaptive feeding, the experimental animals were randomly assigned to eight groups: the normal group, model group, Topical group (L-Topical, M-Topical, H-Topical), and Gavage group (L-Gavage, M-Gavage, H-Gavage), each consisting of five mice. Beginning on the first day of UVB radiation, the mice were treated with IOP according to the detailed administration schedule shown in Fig. 1.

The hairs on the dorsal skin of the mice were shaved, and the skin was exposed to UVB radiation using a sealed box equipped with three 15 W UVB lamps (Sankyo Denki, Japan) for a duration of 6 weeks with a total dose of 3000 mJ/cm^2. The lamps were positioned 25 cm above the mice's back, and the UVB intensity was measured using a UV radiometer. As depicted in Fig. 1, the dose for the first week was 100 mJ/cm^2 for 7 consecutive days. For the second week, the dose was 200 mJ/cm^2 administered once every two days for a total of 4 days. Starting from the third week, the dose was 150 mJ/cm^2 given once every three days for a total of 10 days.

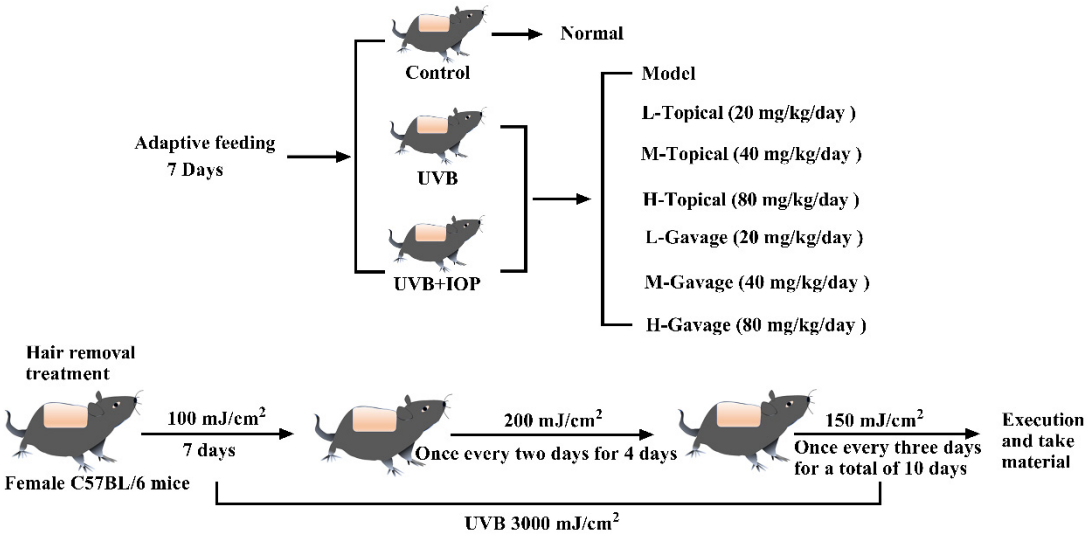

Fig.1 Establishment and administration of the mouse model of photodamage *in vivo*.

2.3 Organ index analysis

At the end of the experiment, the weights of each mouse's liver, spleen, and kidneys were recorded. The organ index calculation formula was as follows:

Organ index = Organ weight (g)/Body weight (g)

2.4 Histological examination

The skin tissue was fixed with 4% paraformaldehyde, dehydrated, embedded in paraffin, and sectioned into a 4 μm thick sample. After paraffin removal, hematoxylin-eosin (H&E) staining and Masson staining were performed, and histopathological changes in the epidermis and collagen fibers were observed by a digital slide scanner (3DHISTCH, Hungary).

2.5 Cell culture and treatment

HaCaT cells, a human epidermal keratinocyte cell line, were purchase from the HAKATA cell bank. HaCaT cells were cultured in Dulbecco's modified Eagle's medium (DMEM, Sigma, D6429-500ML) supplemented with 10% fetal bovine serum (FBS, Lonsera, S711-001S) and 1% penicillin-streptomycin (Biosharp, BL505A) in an atmosphere of 5% CO_2 at 37℃.

To construct an *in vitro* photoaging cell model, HaCaT cells were irradiated with UVB at a dosage of 80 mJ/cm^2. The cells were divided into five groups: the normal group, model group (exposed to UVB irradiation), 0.2 μg/mL IOP group (UVB irradiation with 0.2 μg/mL IOP treatment), 2 μg/mL IOP group (UVB irradiation with 2 μg/mL IOP treatment), and 20 μg/mL IOP group (UVB irradiation with 20 μg/mL IOP treatment).

2.6 Western blot

Skin tissues and cells were subjected to ice bath conditions and treated with RIPA (Thermo Fisher, 87787) reagent for 45 min. After centrifugation (12000 r/min, 10 min at 4℃), the supernatant was collected as a protein sample. The protein concentration was determined using a BCA kit (Beyotime Biotechnology, P0006C). The proteins were separated by SDS-PAGE and transferred onto a preactivated polyvinylidene fluoride membrane (PVDF, Shanghai Universal Biotech, 10600023). The PVDF membranes were blocked with 5% BSA and incubated with the specific primary antibody overnight at 4℃. Subsequently, the PVDF membrane was washed with TBST buffer and incubated with the corresponding horseradish peroxidase-conjugated secondary antibody for 1 h at room temperature. Color development was achieved using enhanced chemiluminescence (ECL) solution (Beyotime Biotechnology, P0018FM), and photographed using a gel imaging system (Tanon 5200Multi). The total gray value of each band was quantified using ImageJ software, and the results were normalized to that of the housekeeping protein GAPDH or ACTB.

2.7 Isolation of total RNA and RT-PCR

Total RNA was extracted from skin tissues using an RNAeasy™ Animal RNA Isolation Kit with a Spin Column (Beyotime Biotechnology, R0027). Total RNA was isolated from HaCaT cells using Trizol reagent (Sangon Biotech, B511311-0100). Complementary DNA synthesis was performed using BeyoRT™ III First Strand cDNA Synthesis Master Mix (Beyotime Biotechnology, D7182M). PCR amplification consisted of 30 cycles of 94℃ for 30 s, 55℃ for 30 s, and 72℃ for 1 min with Easy-Load™ PCR Master Mix (Beyotime Biotechnology, D7255) and primer pairs (Table 1). The total gray level of each band was quantified by ImageJ software. The mRNA expression levels were standardized to the expression of GAPDH.

Table 1. The sequences of primers used in the study

Gene Name	Forward sequences	Reverse sequences
TNF-α	ACCCTCACACTCACAAACCA	ACAAGGTACAACCCATCGGC
IFN-γ	GAGGTCAACAACCCACAGGT	GGGACAATCTCTTCCCCACC
Collagen I	TGAACGTGGTGTACAAGGTC	CCATCTTTACCAGGAGAACCAT
MMP1	CTTCTTCTTGTTGAGCTGGACTC	CTGTGGAGGTCACTGTAGACT
MMP3	CCCTGCAACCGTGAAGAAGA	GACAGCATCCACCCTTGAGT
GAPDH	CAGGTTGTCTCCTGCGACTT	TATGGGGGTCTGGGATGGAA

2.8 ELISA

The Sirt3 concentration in the serum was measured using a Mouse Sirt 3 Elisa Kit (CoiboBio, CB15329-Mu). Briefly, 50 μL of different concentration standards and serum samples were added to a 96-well plate. Subsequently, 100 μL of the enzyme conjugate was added to each well. The plate was then incubated at 37℃ for 60 min. The plate was washed five times with wash solution. Substrate A and B solutions were added to each well, and the plate was incubated in the dark for 15 min. Finally, 50 μL of Stop solution was added to stop the reaction, and the optical density (OD) of each well was measured at a wavelength of 450 nm.

2.9 Autophagy assay

Autophagy was detected according to the instructions of an Autophagy Staining Assay Kit with MDC (Beyotime Biotechnology, C3018M). The cells were washed twice with phosphate buffer (PBS). Next, 1 mL of monodanyl cadaveramide (MDC) staining solution was added to each dish (35 mm). The cell culture dish was placed in a cell culture incubator and incubated at 37℃ for 30 min. Subsequently, each well was washed three times with 1 mL of assay buffer, after which 1 mL of assay buffer was added. Green fluorescence was observed under a fluorescence microscope (Leica), and fluorescence was detected using a fluorescence microplate reader (Tanon, excitation wavelength 335 nm, emission wavelength 512 nm).

2.10 Gut microbiota analysis

DNA was extracted from feces collected from the colons of mice in three groups: normal, model and H-Gavage groups. Thirty nanograms of genomic DNA samples with qualified quality and corresponding fusion primers were configured with a PCR system, and the PCR parameters were set for PCR amplification. The PCR amplification product was purified using Agencourt AMPure XP magnetic beads, dissolved in elution buffer, and labeled, after which the library was constructed. An Agilent 2100 Bioanalyzer was used to measure the extent and concentration of the fragments. The HiSeq platform was selected for sequencing according to the size of the insert.

2.11 Statistical analysis

GraphPad Prism 9.0.1 statistical software (GraphPad, California, USA) was used to determine the significance of the differences in the processed data. The experimental results were presented as the mean ± SD, and the test method was one-way ANOVA. Differences were considered significant at $P < 0.05$.

3. Results

3.1 Effect of IOP on the epidermis of UVB-irradiated mice

In vivo, the organ indices could provide insight into the potential toxic side effects of drugs on mice. In this study, the liver, kidney, and spleen indices of the IOP treatment group were not significantly different from those of the normal group ($P > 0.05$; Fig. 2A-C). To assess the effect of IOP on the epidermis, we performed H&E staining of mouse skin tissue in the UVB-irradiated area (Fig. 2D). The model group exhibited a thickened stratum corneum, an increased number of cell layers, and a significantly thickened epidermis compared to those of the normal group. Moreover, the skin of mice in the model group exhibited

inflammatory cell infiltration. However, compared with those in the model group, the epidermal thickness of the mice in the IOP topical groups and gavage groups were significantly lower.

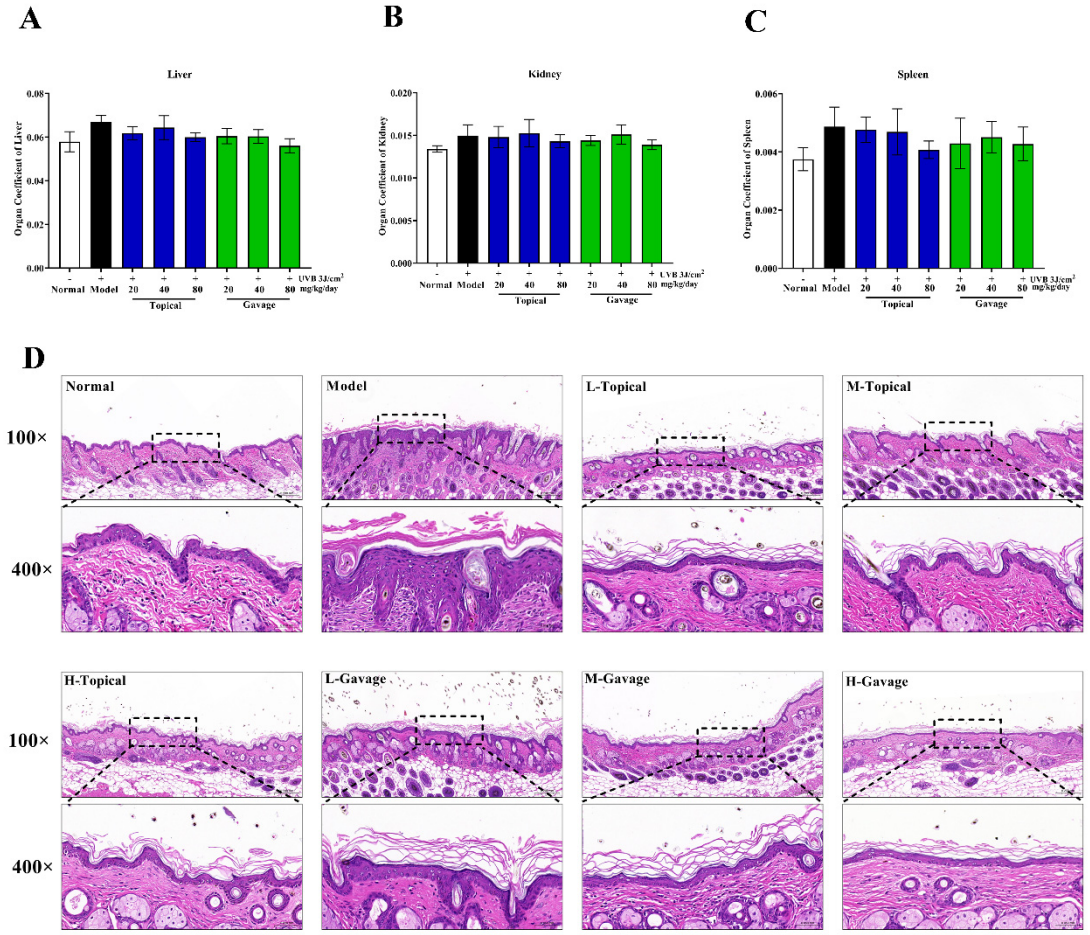

Fig. 2 Effect of IOP on the epidermis of UVB-irradiated mice. (A) Organ indices of the liver. (B) Organ indices of the kidney. (C) Organ indices of the spleen. (D) H&E staining was used to observe the histological changes in the epidermis of the mice (100× and 400×). The data are expressed as the means ± SDs; n=5.

3.2 Effects of IOP on collagen in the skin of UVB-irradiated mice

To investigate the potential inhibitory effect of IOP on collagen degradation caused by UVB radiation, we conducted Masson staining on the skin of the mice (Fig. 3A). In the normal group, the collagen fibers were evenly distributed and tightly arranged. In contrast, the model group exhibited sparse, denatured, and unevenly distributed collagen fibers. However, in both the IOP topical group and the gavage group, the collagen fibers in mouse skin tissue exhibited a significant increase in density, neat arrangement, and relatively uniform distribution compared to those in the model group.

The expression of MMP1 and MMP3 plays a role in the regulation of Collagen I levels in the skin. The mRNA expression of MMP1 and MMP3 in the skin tissue of mice in the model group was significantly greater than that in the skin tissue of the normal group, while the mRNA expression of Collagen I was suppressed ($P < 0.001$; Fig. 3B-C). Conversely, in the IOP treatment groups (both topical and gavage), the mRNA expression of MMP1 and MMP3 was downregulated, and the expression of Collagen I mRNA was significantly upregulated compared to that in the model group (Fig. 3B-C).

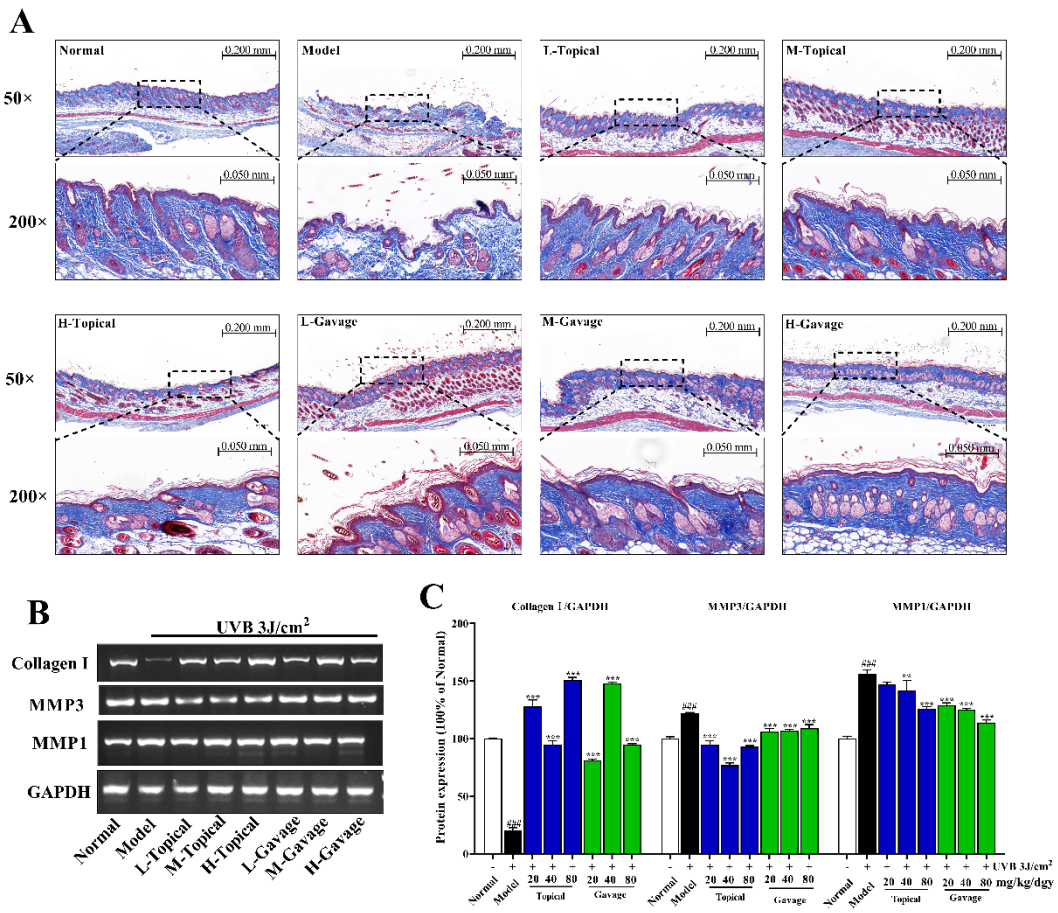

Fig. 3 Effects of IOP on collagen in the skin of UVB-irradiated mice. (A) Skin sections were stained with Massone to observe the distribution and content of collagen fibers in the dermal layer of mice (50× and 200×). (B) RT–PCR results for Collagen I, MMP3 and MMP1. (C) The mRNA levels of Collagen I, MMP3 and MMP1 determined by real-time PCR and referenced to the level of GAPDH. The data were expressed as the means ± SDs; n=3. Compared with the normal group, $^{###}$ $P < 0.001$; compared with the model group, ** $P < 0.01$, *** $P < 0.001$.

3.3 Effects of IOP on inflammation and aging in UVB-irradiated mice

Inflammatory cell infiltration in the model group was observed through H&E staining, and the level of inflammation in the skin tissue was measured. The expression of TNF-α and IFN-γ mRNA in the skin tissue of the model group was significantly greater than that in the skin tissue of the normal group ($P < 0.001$; Fig. 4A-C). However, in all IOP treatment groups except for the L-Topical group, TNF-α and IFN-γ mRNA expression was significantly inhibited ($P < 0.001$; Fig. 4A-C).

Subsequently, we examined age-related indicators in the skin tissue (Fig. 4D-F). After UVB irradiation, the expression of the intracellular aging-related factors P53 and P21 in the model group increased significantly compared to that in the normal group ($P < 0.001$), resulting in cell senescence and exacerbation of photodamage. This finding indicates that cellular senescence worsens photoaging. However, after IOP administration, the protein expression of P53 and P21 in the smearing group was significantly lower than that in the model group ($P < 0.001$). Similarly, the protein expression of P53 and P21 in the M-Gavage group and the H-Gavage group was significantly downregulated ($P < 0.001$).

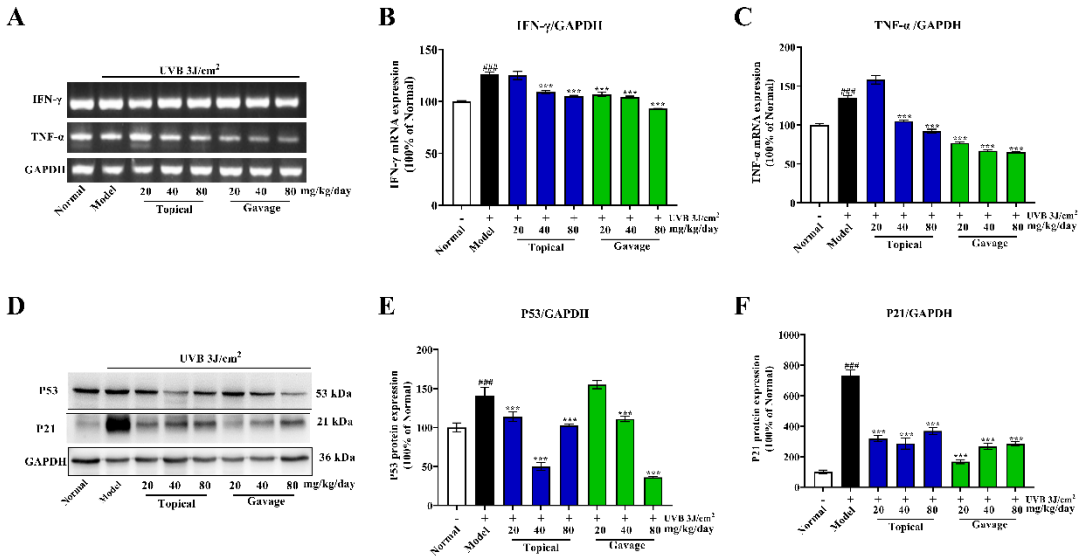

Fig. 4 Effects of IOP on inflammation and aging in UVB-irradiated mice. (A) RT–PCR results for IFN-γ and TNF-α. The mRNA levels of (B) IFN-γ and (C) TNF-α determined by real-time PCR and referenced to the level of GAPDH. (F) Western blot analysis of P53 and P21. The levels of (G) P53 and (H) P21 were presented as the ratio (in percentage) of the normal group and were and referenced to the level of GAPDH. The data are expressed as the means ± SDs; n=3. Compared with the normal group, $^{###}$ $P < 0.001$; compared with the model group, *** $P < 0.001$.

3.4 Effect of IOP on autophagy levels in UVB-irradiated mice

Sirt3 plays a crucial role in maintaining mitochondrial integrity[25]. To investigate the potential regulatory effect of Sirt3 on IOP, we examined the serum Sirt3 concentration and the Sirt3 protein level in the bare skin tissue (Fig. 5A-C). Compared to those in the normal group, the serum Sirt3 content in the model group was slightly lower, with a 59% decrease in Sirt3 protein expression. However, the other IOP treatment groups, except for the L-Topical group, exhibited an upward trend in the expression of Sirt3 in both the serum and skin. The expression of proteins related to the mitophagy pathway, Foxo3a, PINK1, and Parkin, in the skin of mice in the model group was downregulated (Fig. 5D-E). Conversely, the H-Gavage group exhibited significant upregulation of Foxo3a, PINK1, and Parkin protein expression in the UVB radiation region ($P <$ 0.001).

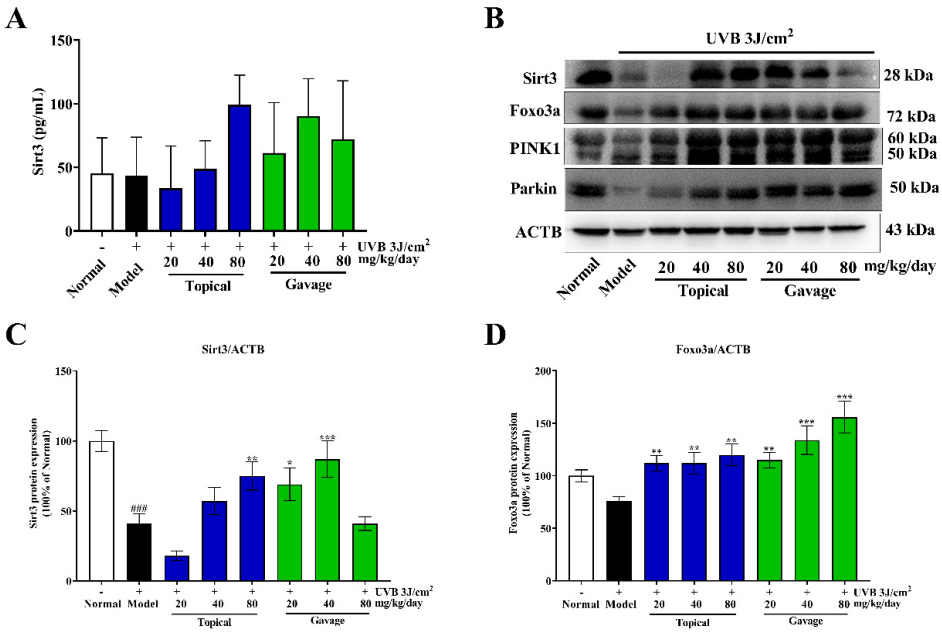

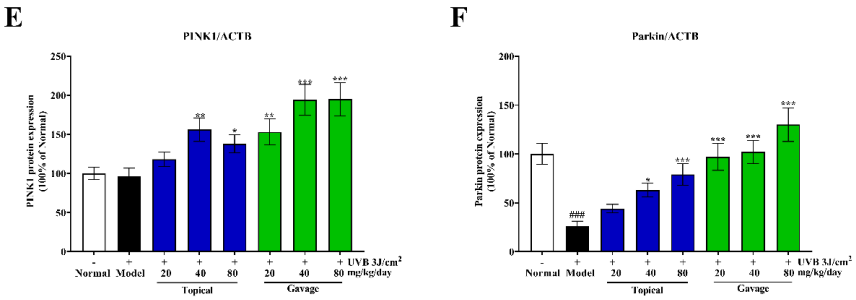

Fig. 5 Effect of IOP on autophagy levels in UVB-irradiated mice. (A) ELISA of Sirt3 in mouse serum. (B) Western blot analysis of Sirt3, Foxo3a, PINK1 and Parkin. The quantification of (C) Sirt3, (D) Foxo3a, (E) PINK1 and (F) Parkin were presented as the ratio (in percentage) of the normal group and referenced to ACTB. The data are expressed as the means ± SDs; n=3. Compared with the normal group, $^{###}$ $P < 0.001$; compared with the model group, * $P < 0.05$, ** $P < 0.01$, *** $P < 0.001$.

3.5 Effect of IOP on gut microbes in UVB-irradiated mice

The alpha diversity indices were determined using the Chao 1, Shannon and Simpson indices. The Chao1 and Shannon indices were greater in the normal group and H-Gavage group than in the model group (Fig. 6A, B). On the other hand, the Simpson index was lower in the normal group and H-Gavage group than in the model group (Fig. 6C).

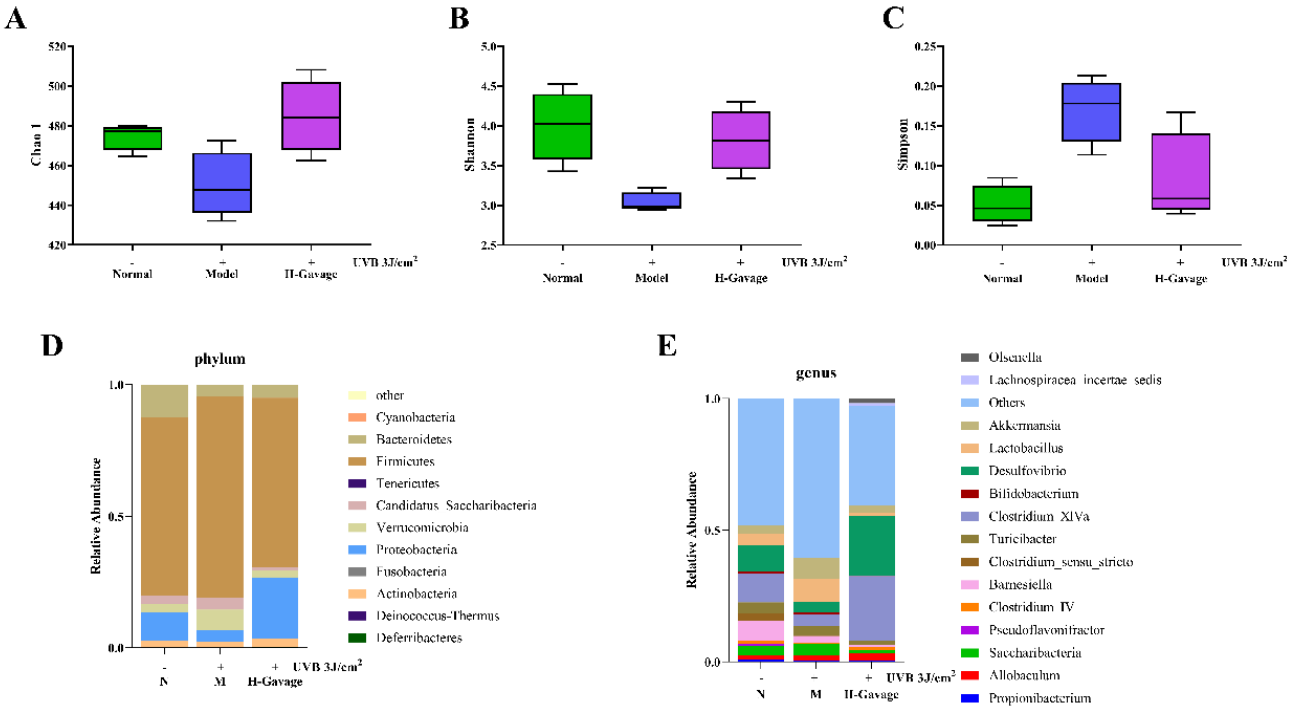

Fig. 6 Effect of IOP on gut microbes in UVB-irradiated mice. (A) Chao 1 index. (B) Shannon index. (C) Simpson index. Histogram of the gut microbial compositions at the (D) phylum and (E) family levels.

Regarding the richness of the microbial species, the dominant genera were *Firmicutes, Bacteroidetes, Proteobacteria, Verrucomicrobia, Candidatus_Saccharibacteria,* and *Actinobacteria* (Fig. 6D). Among the gut microorganisms of mice in the normal group, the F/B ratio between the phylum Firmicutes and the Bacteroides phylum was 5.45, and this ratio increased to 17.45 in the model group. In the H-Gavage group, the ratio of the phylum Firmicutes to the phylum Bacteroides was 12.852, a decrease of 4.598 compared with that in the model group. At the subordinate level, compared with that in the normal group, the richness of

Clostridium_XlVa in the model group was reduced by 7%, the richness of *Desulfovibrio* was reduced by 6%, and the richness of *Barnesiella* was reduced by 5%. *Akkermansia* richness was revised by 5%, and *Lactobacillus* richness was revised by 5%. Compared to that in the model group, the richness of *Clostridium_XlVa* in the drug group was increased by 20%, and the richness of *Desulfovibrio* was increased by 19%. However, the richness of *Lactobacillus* was reduced by 7%, and *the* richness of *Akkermansia* was reduced by 5%.

3.6 Effect of IOP on autophagy levels in UVB-irradiated cells

The protein expression of Sirt3 in the cells in the model group was significantly lower than that in the normal group after UVB irradiation ($P < 0.001$; Fig. 7A-B). The protein expression of Sirt3 in each group after drug administration basically showed an upward trend compared to that in the model group (Fig. 7A-B). Additionally, compared with those in the normal group, the expression of FOXO3a, PINK1 and Parkin in the model group was lower. However, in the IOP treatment group, the expression of the Foxo3a, PINK1 and Parkin proteins increased in the 2 μg/mL IOP group, and these proteins were significantly upregulated ($P < 0.001$; Fig. 7C-D). In addition, the protein expression of Bnip3 (Bcl-2/adenovirus E1B 19-kDa-interacting protein 3) reflects autophagy levels. Compared with that in the normal group, the protein expression of Bnip3 in the model group was downregulated. However, there was a clear upregulation trend of the Bnip3 protein in the 2 μg/mL IOP group (Fig. 7E-F).

As shown in Fig. 7G, the normal group represents the baseline level of autophagy without UVB irradiation. To inhibit autophagy, 3-Methyladenine (3-MA) was used. Compared to those in the normal group, the 3-MA group exhibited a decrease in fluorescence intensity. Similarly, the Model group showed a reduction in fluorescence spots and weakened autophagy intensity. In the 20 μg/mL IOP dose group, there was a significant increase in the number of MDC-positive cells and a corresponding increase in fluorescence intensity.

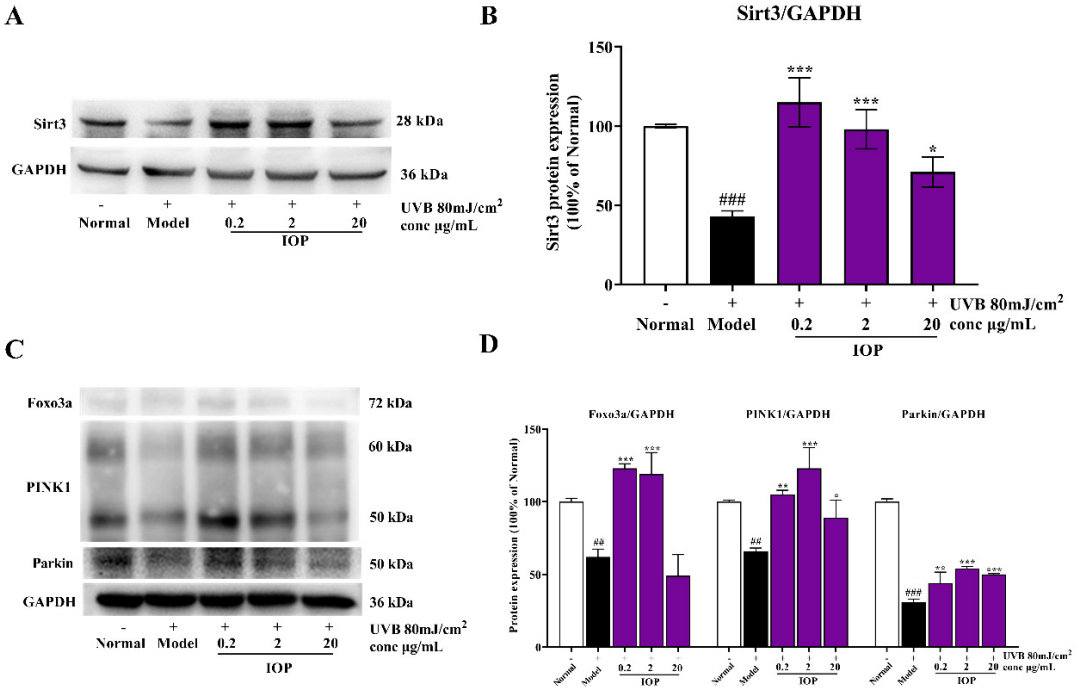

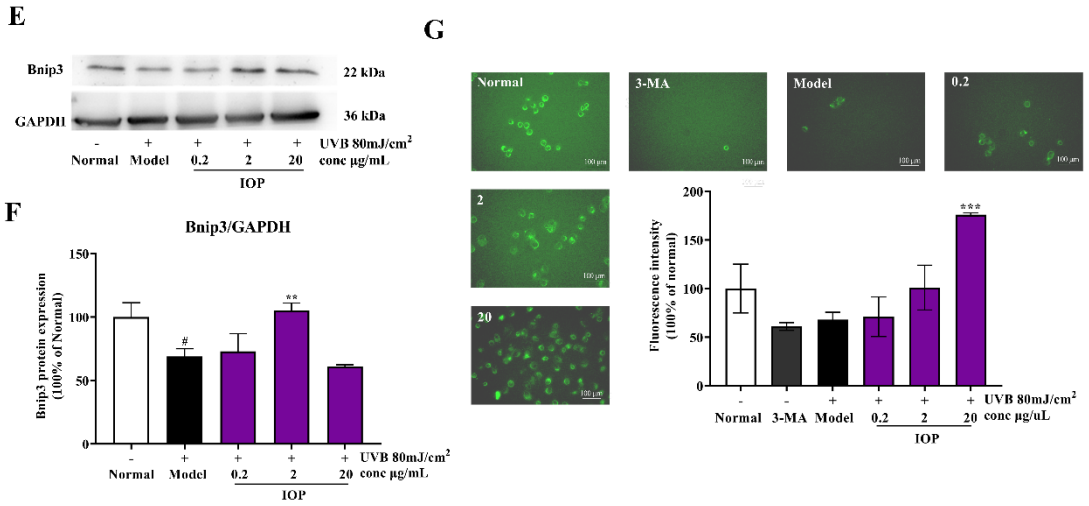

Fig. 7 Effect of IOP on autophagy levels in UVB-irradiated cells. (A) Western blot analysis of Sirt3. (B) Quantification of Sirt3 was presented as the ratio (in percentage) of the normal group and referenced to GAPDH. (C) Western blot analysis of Foxo3a, PINK1 and Parkin. (D) The Foxo3a, PINK1 and Parkin levels are presented as the ratio (in percentage) of the normal group and referenced to the GAPDH level. (E) Western blot analysis of Bnip3. (F) Quantification of Bnip3 expression was presented as the ratio (in percentage) of the normal group and referenced to the GAPDH level. (G) MDC-positive cells and fluorescence intensity were presented as the ratio (in percentage) to that of the normal group. The data are expressed as the means ± SDs; n=3. Compared with those in the normal group, $^{\#}P < 0.05$, $^{\#\#}P < 0.01$, and $^{\#\#\#}P < 0.001$; compared with those in the model group, $^{*}P < 0.05$, $^{*}P < 0.01$, and $^{***}P < 0.001$.

4. Discussion

IOP possesses various biological activities, especially strong antioxidant and anti-inflammatory properties[26-29]. Our previous study revealed that IOP can effectively prevent oxidative stress and apoptosis in HaCaT cells caused by UVB radiation. In addition, UVB radiation led to a decrease in the mitochondrial membrane potential of HaCaT cells and a decrease in the expression of genes associated with autophagy, such as Beclin-1 and LC3. However, these detrimental effects were alleviated upon IOP treatment[24]. Based on these findings, we propose that IOP can potentially alleviate UVB-induced mitochondrial dysfunction and induce autophagy, suggesting that IOP is a promising approach for the treatment of skin photodamage.

Collagen, the main component of the extracellular matrix (ECM), is susceptible to degradation due to UV radiation, which can accelerate the skin aging process. This degradation is caused by the upregulation of the MMP1 and MMP3 proteins[30-32]. Prolonged exposure to UVB radiation also leads to increased expression of aging markers, such as p53 and p21, in human keratinocytes. These markers further contribute to the secretion of aging-related factors such as TNF-α[33]. In our study, we discovered that IOP can mitigate the degradation of collagen fibers caused by UVB radiation. This effect is achieved by inhibiting the expression of MMP1 and MMP3. Furthermore, IOP also suppresses inflammatory factor and senescence-related protein expression. These findings suggest that IOP has a potential role in alleviating skin photodamage.

Autophagy is a cellular process that maintains homeostasis and eliminates damaged cellular components to promote cell survival and adaptive responses. Dysfunction in autophagy contributes to UV-induced skin cell damage, leading to photoaging and photodamage[34]. Previous studies have indicated that increasing autophagy can alleviate skin photodamage [34-37]. Sirt3, a mitochondrial deacetylase enzyme, plays a role in regulating mitochondrial quality and mitophagy by modifying protein acetylation. Increased expression of

Sirt3 has been shown to activate key proteins involved in mitochondrial autophagy, including FOXO3a, PINK1, and Parkin[38, 39]. By activating the Foxo3a/Parkin pathway, Sirt3 stimulates cellular mitochondrial autophagy, thereby improving TNF-α-induced psoriasis in HaCaT cells[40]. Considering that UVB radiation can also induce mitochondrial dysfunction, we hypothesized that the Sirt3-PINK1/Parkin pathway could alleviate skin photodamage. Through *in vivo* and *in vitro* experiments, we demonstrated that UVB radiation reduces the expression of Sirt3 and its downstream proteins. As expected, IOP increased the expression of Sirt3 and activated the Foxo3a/PINK1-Parkin signaling pathway, thereby enhancing mitophagy. These findings suggest that Sirt3 could serve as a potential target for treating photodamage.

The intestine and skin are organs that are rich in blood vessels and nerves, and they have important effects on the immune system and neuroendocrine system[41]. These organs are closely connected to each other through a pathway known as the gut-skin axis[42]. Recent studies have shown that various skin diseases, such as acne, specific dermatitis, and psoriasis, are associated with an imbalance of the intestinal flora[43-46]. The F/B ratio, which is often used as an indicator of microbial imbalance, is linked to intestinal dermatology[47]. In the present study, we observed that exposure to UVB radiation caused dysregulation of gut microbes, an increase in the F/B ratio, and a decrease in gut microbial diversity. The relative abundances of *Clostridium_XlVa, Desulfovibrio,* and *Barnesiella*, which are important for protecting the intestinal barrier and alleviating intestinal dysfunction, were significantly reduced in the photodamage model[48, 49]. Our study proved that IOP can regulate gut microbes in photodamaged mice.

5. Conclusions

In our study, we investigated the effects of UVB radiation on the skin and evaluated the potential benefits of IOP treatment. We found that UVB radiation caused several changes in the skin, such as epidermal thickening, inflammation, aging, and collagen fiber degradation. However, when the mice in the IOP treatment group were exposed to UVB radiation, we observed that their skin epidermis became thinner and that the number of collagen fibers increased. Moreover, the expression of genes related to inflammation and aging decreased in the IOP treatment group, suggesting a decrease in the photoaging process. Additionally, IOP treatment showed promising results in alleviating dysbiosis of the intestinal flora in mice with photodamage. Both *in vitro* and *in vivo* experiments revealed that IOP increased the expression of Sirt3 after UVB radiation and activated the Foxo3a/PINK1-Parkin pathway, which enhanced mitochondrial autophagy and provided protection against UVB damage.

Conflicts of interest

The authors declared no conflict of interest.

Acknowledgments

This work was supported by the National Natural Science Foundation of China (No. 82004027) and the Fundamental Research Funds for the Central Universities (JUSRP11961).

References

[1] R. Geng, S. G. Kang, K. Huang, et al., alpha-Ionone protects against UVB-induced photoaging in epidermal keratinocytes, Chin Herb Med. 15 (2023) 132-138. https://doi.org/10.1016/j.chmed.2022.09.003.

[2] L. L. Guan, H. W. Lim, T. F. Mohammad, Sunscreens and Photoaging: A Review of Current Literature, Am J Clin Dermatol. 22 (2021) 819-828. https://doi.org/10.1007/s40257-021-00632-5.

[3] J. Mu, H. Ma, H. Chen, et al., Luteolin Prevents UVB-Induced Skin Photoaging Damage by Modulating SIRT3/ROS/MAPK Signaling: An in vitro and in vivo Studies, Front Pharmacol. 12 (2021) 728261. https://doi.org/10.3389/fphar.2021.728261.

[4] L. A. Videla, A. Mariman, B. Ramos, et al., Standpoints in mitochondrial dysfunction: Underlying mechanisms in search of therapeutic strategies, Mitochondrion. 63 (2022) 9-22. https://doi.org/10.1016/j.mito.2021.12.006.

[5] Y. Luo, J. Ma, W. Lu, The Significance of Mitochondrial Dysfunction in Cancer, Int J Mol Sci. 21 (2020) https://doi.org/10.3390/ijms21165598.

[6] C. Li, Y. Zhu, W. Liu, et al., Impaired mitophagy causes mitochondrial DNA leakage and STING activation in ultraviolet B-irradiated human keratinocytes HaCaT, Arch Biochem Biophys. 737 (2023) 109553. https://doi.org/10.1016/j.abb.2023.109553.

[7] J. Guo, W. C. Chiang, Mitophagy in aging and longevity, IUBMB Life. 74 (2022) 296-316. https://doi.org/10.1002/iub.2585.

[8] S. K. Ghosh-Choudhary, J. Liu, T. Finkel, The role of mitochondria in cellular senescence, FASEB J. 35 (2021) e21991. https://doi.org/10.1096/fj.202101462R.

[9] Y. Lu, Z. Li, S. Zhang, et al., Cellular mitophagy: Mechanism, roles in diseases and small molecule pharmacological regulation, Theranostics. 13 (2023) 736-766. https://doi.org/10.7150/thno.79876.

[10] X. Liu, C. Yang, Y. Deng, et al., Polygoni Multiflori Radix Preparat Delays Skin Aging by Inducing Mitophagy, Biomed Res Int. 2021 (2021) 5847153. https://doi.org/10.1155/2021/5847153.

[11] J. Hu, T. Kan, X. Hu, Sirt3 regulates mitophagy level to promote diabetic corneal epithelial wound healing, Exp Eye Res. 181 (2019) 223-231. https://doi.org/10.1016/j.exer.2019.02.011.

[12] O. A. Ahmedy, T. M. Abdelghany, M. E. A. El-Shamarka, et al., Apigenin attenuates LPS-induced neurotoxicity and cognitive impairment in mice via promoting mitochondrial fusion/mitophagy: role of SIRT3/PINK1/Parkin pathway, Psychopharmacology (Berl). 239 (2022) 3903-3917. https://doi.org/10.1007/s00213-022-06262-x.

[13] J. Zhang, H. Xiang, J. Liu, et al., Mitochondrial Sirtuin 3: New emerging biological function and therapeutic target, Theranostics. 10 (2020) 8315-8342. https://doi.org/10.7150/thno.45922.

[14] P. Gupta, G. Sharma, A. Lahiri, et al., FOXO3a acetylation regulates PINK1, mitophagy, inflammasome activation in murine palmitate-conditioned and diabetic macrophages, Journal of Leukocyte Biology. 111 (2022) 611-627. https://doi.org/10.1002/jlb.3a0620-348rr.

[15] J. Hu, T. Liu, F. Fu, et al., Omentin1 ameliorates myocardial ischemia-induced heart failure via SIRT3/FOXO3a-dependent mitochondrial dynamical homeostasis and mitophagy, Journal of Translational Medicine. 20 (2022) https://doi.org/10.1186/s12967-022-03642-x.

[16] W. Yu, B. Gao, N. Li, et al., Sirt3 deficiency exacerbates diabetic cardiac dysfunction: Role of Foxo3A-Parkin-mediated mitophagy, Biochimica et Biophysica Acta (BBA) - Molecular Basis of Disease. 1863 (2017) 1973-1983. https://doi.org/10.1016/j.bbadis.2016.10.021.

[17] K. Sun, X. Jing, J. Guo, et al., Mitophagy in degenerative joint diseases, Autophagy. 17 (2021) 2082-2092. https://doi.org/10.1080/15548627.2020.1822097.

[18] T. Xin, C. Lu, SirT3 activates AMPK-related mitochondrial biogenesis and ameliorates sepsis-induced myocardial injury, Aging (Albany NY). 12 (2020) 16224-16237. https://doi.org/10.18632/aging.103644.

[19] T. Zhang, J. Liu, S. Shen, et al., SIRT3 promotes lipophagy and chaperon-mediated autophagy to protect hepatocytes against lipotoxicity, Cell Death Differ. 27 (2020) 329-344. https://doi.org/10.1038/s41418-019-0356-z.

[20] K. A. Szychowski, B. Skora, T. Pomianek, et al., Inonotus obliquus - from folk medicine to clinical use, J Tradit Complement Med. 11 (2021) 293-302. https://doi.org/10.1016/j.jtcme.2020.08.003.

[21] M. E. Balandaykin, I. V. Zmitrovich, Review on Chaga Medicinal Mushroom, Inonotus obliquus (Higher Basidiomycetes):

Realm of Medicinal Applications and Approaches on Estimating its Resource Potential, Int J Med Mushrooms. 17 (2015) 95-104. https://doi.org/10.1615/intjmedmushrooms.v17.i2.10.

[22] Y. Lu, Y. Jia, Z. Xue, et al., Recent Developments in Inonotus obliquus (Chaga mushroom) Polysaccharides: Isolation, Structural Characteristics, Biological Activities and Application, Polymers (Basel). 13 (2021) https://doi.org/10.3390/polym13091441.

[23] L. Jingjing, L. Pei, L. Jun, Intervention effect of Inonotus obliquus on UVB-induced photoaging in HaCaT cells Highlights of Sciencepaper Online. 14 (2021) 391-401.

[24] J. Lin, Y.-y. Lu, H.-y. Shi, et al., Chaga Medicinal Mushroom, Inonotus obliquus (Agaricomycetes) Polysaccharides Alleviate Photoaging via Regulating Nrf2 Pathway and Autophagy, International Journal of Medicinal Mushrooms. 25 (2023) 49-64.

[25] L. Papa, D. Germain, SirT3 regulates the mitochondrial unfolded protein response, Mol Cell Biol. 34 (2014) 699-710. https://doi.org/10.1128/MCB.01337-13.

[26] J. Zhang, S. Cheng, J. Liang, et al., Polysaccharide from fermented mycelium of Inonotus obliquus attenuates the ulcerative colitis and adjusts the gut microbiota in mice, Microb Pathog. 177 (2023) 105990. https://doi.org/10.1016/j.micpath.2023.105990.

[27] L. Su, C. Xin, J. Yang, et al., A polysaccharide from Inonotus obliquus ameliorates intestinal barrier dysfunction in mice with type 2 diabetes mellitus, Int J Biol Macromol. 214 (2022) 312-323. https://doi.org/10.1016/j.ijbiomac.2022.06.071.

[28] Y. Han, S. Nan, J. Fan, et al., Inonotus obliquus polysaccharides protect against Alzheimer's disease by regulating Nrf2 signaling and exerting antioxidative and antiapoptotic effects, International Journal of Biological Macromolecules. 131 (2019) 769-778. https://doi.org/10.1016/j.ijbiomac.2019.03.033.

[29] C. Wang, R. K. Santhanam, X. Gao, et al., Preparation, characterization of polysaccharides fractions from Inonotus obliquus and their effects on α-amylase, α-glucosidase activity and H2O2-induced oxidative damage in hepatic L02 cells, Journal of Functional Foods. 48 (2018) 179-189. https://doi.org/10.1016/j.jff.2018.07.024.

[30] H. Y. Jung, J. C. Shin, S. M. Park, et al., Pinus densiflora extract protects human skin fibroblasts against UVB-induced photoaging by inhibiting the expression of MMPs and increasing type I procollagen expression, Toxicol Rep. 1 (2014) 658-666. https://doi.org/10.1016/j.toxrep.2014.08.010.

[31] Z. Xiao, S. Yang, J. Chen, et al., Trehalose against UVB-induced skin photoaging by suppressing MMP expression and enhancing procollagen I synthesis in HaCaT cells, Journal of Functional Foods. 74 (2020) https://doi.org/10.1016/j.jff.2020.104198.

[32] E.-M. Noh, G. Lee, C.-H. Lim, et al., Protective effects of Evodiae Fructus extract against ultraviolet-induced MMP-1 and MMP-3 expression in human dermal fibroblasts, Journal of Herbal Medicine. 35 (2022) https://doi.org/10.1016/j.hermed.2022.100586.

[33] E. Fitsiou, T. Pulido, J. Campisi, et al., Cellular Senescence and the Senescence-Associated Secretory Phenotype as Drivers of Skin Photoaging, J Invest Dermatol. 141 (2021) 1119-1126. https://doi.org/10.1016/j.jid.2020.09.031.

[34] J. Ma, Y. Teng, Y. Huang, et al., Autophagy plays an essential role in ultraviolet radiation-driven skin photoaging, Front Pharmacol. 13 (2022) 864331. https://doi.org/10.3389/fphar.2022.864331.

[35] D. Hao, X. Wen, L. Liu, et al., Sanshool improves UVB-induced skin photodamage by targeting JAK2/STAT3-dependent autophagy, Cell Death Dis. 10 (2019) 19. https://doi.org/10.1038/s41419-018-1261-y.

[36] M. Wang, P. Charareh, X. Lei, et al., Autophagy: Multiple Mechanisms to Protect Skin from Ultraviolet Radiation-Driven Photoaging, Oxid Med Cell Longev. 2019 (2019) 8135985. https://doi.org/10.1155/2019/8135985.

[37] A. Sample , Y. Y. He, Autophagy in UV Damage Response, Photochem Photobiol. 93 (2017) 943-955. https://doi.org/10.1111/php.12691.

[38] Y. Mishra, R. K. Kaundal, Role of SIRT3 in mitochondrial biology and its therapeutic implications in neurodegenerative disorders, Drug Discov Today. 28 (2023) 103583. https://doi.org/10.1016/j.drudis.2023.103583.

[39] L. Huang, T. Yao, J. Chen, et al., Effect of Sirt3 on retinal pigment epithelial cells in high glucose through Foxo3a/PINK1-Parkin pathway mediated mitophagy, Exp Eye Res. 218 (2022) 109015. https://doi.org/10.1016/j.exer.2022.109015.

[40] M. Yanli, W. Yu, L. Yuzhen, Elevated SIRT3 Parkin-dependently activates cell mitophagy to ameliorate TNF-alpha-induced psoriasis-related phenotypes in HaCaT cells through deacetylating FOXO3a for its activation, Arch Dermatol Res. 315 (2023)

847-857. https://doi.org/10.1007/s00403-022-02453-w.

[41] I. Salem, A. Ramser, N. Isham, et al., The Gut Microbiome as a Major Regulator of the Gut-Skin Axis, Front Microbiol. 9 (2018) 1459. https://doi.org/10.3389/fmicb.2018.01459.

[42] A. Y. Thye, Y. R. Bah, J. W. Law, et al., Gut-Skin Axis: Unravelling the Connection between the Gut Microbiome and Psoriasis, Biomedicines. 10 (2022) https://doi.org/10.3390/biomedicines10051037.

[43] I. Olejniczak-Staruch, M. Ciazynska, D. Sobolewska-Sztychny, et al., Alterations of the Skin and Gut Microbiome in Psoriasis and Psoriatic Arthritis, Int J Mol Sci. 22 (2021) https://doi.org/10.3390/ijms22083998.

[44] S. Y. Lee, E. Lee, Y. M. Park, et al., Microbiome in the Gut-Skin Axis in Atopic Dermatitis, Allergy Asthma Immunol Res. 10 (2018) 354-362. https://doi.org/10.4168/aair.2018.10.4.354.

[45] P. Sanchez-Pellicer, L. Navarro-Moratalla, E. Nunez-Delegido, et al., Acne, Microbiome, and Probiotics: The Gut-Skin Axis, Microorganisms. 10 (2022) https://doi.org/10.3390/microorganisms10071303.

[46] Y. Su, F. Zhang, W. Qin, et al., "Gut-skin"axis: understanding psoriasis from the gut, Pharmazie. 76 (2021) 523-527. https://doi.org/10.1691/ph.2021.1694.

[47] L. Qi, H. Mao, X. Lu, et al., Cinnamaldehyde Promotes the Intestinal Barrier Functions and Reshapes Gut Microbiome in Early Weaned Rats, Front Nutr. 8 (2021) 748503. https://doi.org/10.3389/fnut.2021.748503.

[48] Y. Gu, X. Qin, G. Zhou, et al., Lactobacillus rhamnosus GG supernatant promotes intestinal mucin production through regulating 5-HT4R and gut microbiota, Food Funct. 13 (2022) 12144-12155. https://doi.org/10.1039/d2fo01900k.

[49] X. Wang, C. Yu, X. Liu, et al., Fenofibrate Ameliorated Systemic and Retinal Inflammation and Modulated Gut Microbiota in High-Fat Diet-Induced Mice, Front Cell Infect Microbiol. 12 (2022) 839592. https://doi.org/10.3389/fcimb.2022.839592.